Journal of Macromolecular Science, Part B
Physics

ISSN: (Print) (Online) Journal homepage: https://www.tandfonline.com/loi/lmsb20

Tailoring the Microstructural, Optical, and Magnetic Properties of $MgFe_2O_4$ Nanoparticles Capped Polyethylene Glycol Through a Bio-Inspired Method

Abeeha Batool, Samson O. Aisida, Ijeh Rufus, Arshad Mahmood, Ishaq Ahmad, Ting-kai Zhao & Fabian I. Ezema

To cite this article: Abeeha Batool, Samson O. Aisida, Ijeh Rufus, Arshad Mahmood, Ishaq Ahmad, Ting-kai Zhao & Fabian I. Ezema (2022): Tailoring the Microstructural, Optical, and Magnetic Properties of $MgFe_2O_4$ Nanoparticles Capped Polyethylene Glycol Through a Bio-Inspired Method, Journal of Macromolecular Science, Part B, DOI: 10.1080/00222348.2022.2116916

To link to this article: https://doi.org/10.1080/00222348.2022.2116916

Published online: 12 Sep 2022.

JOURNAL OF MACROMOLECULAR SCIENCE, PART B
https://doi.org/10.1080/00222348.2022.2116916

Tailoring the Microstructural, Optical, and Magnetic Properties of $MgFe_2O_4$ Nanoparticles Capped Polyethylene Glycol Through a Bio-Inspired Method

Abeeha Batool[a,b], Samson O. Aisida[b,c,d,e,f], Ijeh Rufus[g], Arshad Mahmood[h], Ishaq Ahmad[b,f], Ting-kai Zhao[f,i], and Fabian I. Ezema[c,d,e]

[a]Centre for High Energy Physics, University of the Punjab, Lahore, Pakistan; [b]National Centre for Physics, Quaid-i-Azam University Campus, Islamabad, Pakistan; [c]Department of Physics and Astronomy, University of Nigeria Nsukka, Nsukka, Nigeria; [d]Nanosciences African Network (NANOAFNET), iThemba LABS-National Research, Johannesburg, South Africa; [e]UNESCO-UNISA Africa Chair in Nanosciences/Nanotechnology, College of Graduate Studies, University of South Africa (UNISA), Pretoria, South Africa; [f]NPU-NCP Joint International Research Center on Advanced Nanomaterials and Defects Engineering, Northwestern Polytechnical University, Xi'an, China; [g]Department of Physics, University of Delta, Agbor, Nigeria; [h]Department of Physics, National Institute of Lasers and Optronics (NILOP), Islamabad, Pakistan; [i]School of Materials Science & Engineering, Northwestern Polytechnical University, Xi'an, China

ABSTRACT
Ferrite materials have found applications in numerous areas, chiefly for hyperthermia in cancer therapy, targeted drug delivery and photodegradation. In this work, magnesium ferrite nanoparticles (MgFNPs) were formulated using polyethylene glycol (PEG) as a capping agent to tailor the properties and heighten the biocompatibility for suitable biomedical applications. The characterization results clearly showed the effect of PEG tailoring the properties of the formulated MgFNPs. A crystallite size with a value between 16 and 91 nm was determined from the X-ray diffraction (XRD) analysis. The scanning electron microscopy (SEM) analysis showed particles of spherical shape for all the samples and the particle size was enhanced as the concentration of PEG increased. The vibrating sample magnetometer (VSM) showed a ferromagnetic nature for the samples with reduced saturation magnetization as the concentration of PEG was increased. The PEG concentration heightened the properties of the sample and can be highly optimized for suitable biomedical applications.

ARTICLE HISTORY
Received 24 February 2022
Accepted 12 August 2022

KEYWORDS
ferrite materials; magnesium nanoparticles; microstructural properties; optical properties; polyethylene glycol

1. Introduction

Nanotechnology is an emerging branch of science that describes the properties of incredibly small size aggregate of molecules and atoms round about 1–100 nm and it's one of the most exciting and fast-moving current areas of science.[1] This multidisciplinary field involves a large number of chemists, physicists, material scientists and engineers analyzing the materials at the nanoscale. Nanotechnology via nanomaterials has found a myriad range of applications in the fields of nanomedicine, biomaterials and

CONTACT Samson O. Aisida samson.aisida@unn.edu.ng Department of Physics and Astronomy, University of Nigeria Nsukka, Nsukka 410001, Nigeria.

energy production.[1] Spinel ferrites, with the general formula often expressed as MFe_2O_3 (M = Co, Mg, Ni, Mn, etc.) in which M^+ ions are placed at the tetrahedral sites (A) and Fe^+ are placed at octahedral sites (B) enclosed by oxygen ions, have received tremendous attention.[2] The distribution of M^+ ions at A-sites and Fe^+ ions at B-sites has shown some influence on the magnetic properties of MFe_2O_4; we suggest it can be controlled by suitable thermal treatment and control of the particle size.[3–5]

Magnesium ferrite ($MgFe_2O_3$), a spinel-type ferrite, has been considered a very valuable material due to its wide variety of attractive electrical, optical and magnetic properties. In addition, such ferrites have demonstrated more ingenious advantages, such as being a heterogeneous catalyst,[6] photo-catalyst,[7] oxygen sensor,[4] and liquefied petroleum gas (LPG) sensor,[5] as compared to other ferrite nanomaterials. The magnetic properties variation with the particle size promote its uses for the treatment of indigenous hyperthermia[8] and drug delivery,[9] gas sensing,[10] magnetic resonance imaging (MRI)[11] applications, etc. In recent years, extensive investigations have already been carried out for the synthesis of magnesium ferrites with developed magnetic and physical properties.[12,13]

The substitution of various cations can modify the properties of $MgFe_2O_3$. In order to understand the effect of the cations distribution in material applications, the synthesis of the nanomaterials must be done based on high purity materials. Generally, solid-state reactions are used to synthesize magnesium ferrites at high temperatures above 1000 °C, which easily produce agglomerated particles having irregular shapes.[14,15] In recent years, numerous wet chemical techniques have been proposed to prepare magnesium ferrites nanoparticles using sol-gel,[16–18] solution combustion,[19,20] polymeric precursor,[21] reverse micelle,[22] microemulsion[23] and hydrothermal procedures[24–26] and biogenic/biosynthesis,[27] etc. Among these methods, biogenic/biosynthesis is one of the most approachable contemporary techniques for producing various nanoparticles. This method involves using an organic solvent, such as urea, and biopolymers, polymers, plant extract, etc., as a chelating agent. Polyethylene glycol (PEG) is a hygroscopic macromolecule with a well-defined structure. It has good water and organic solvent solubility and low toxicity, is highly biocompatible and is biodegradable. Owing to all these properties, PEG has a wide range of applications in the chemical, biochemical, and biotechnological industries.[28]

Herein a bio-inspired synthesis protocol was used to produce PEG-MgFNPs by varying the concentrations of PEG as a potential capping agent to tailor the microstructural, optical and magnetic properties and enhance the biocompatibility of the sample. Based on the various characterizations, the properties of the samples were enhanced and they were made suitable for biomedical applications.

2. Materials and experimentation

Analytical grade $Mg(NO_3)_2 \cdot 6H_2O$ and $Fe(NO_3)_3 \cdot 9H_2O$ precursors, commercial products of Sigma Adrich Co. in Pakistan were used without further purification. PEG (6000 g/mol) was used as a capping agent. The synthesis procedures were conducted in double distilled water (DDW). Magnesium ferrites nanoparticles were synthesized by a biogenic scheme using a stoichiometric quantity of magnesium nitrates and iron nitrate without

Table 1. Composition of the samples.

Sample	$Mg(NO_3)_2$ (g)	$Fe(NO_3)_3$ (g)	PEG (g)
T_1	0.97	4.04	0.0
T_2	0.97	4.04	3.0
T_3	0.97	4.04	6.0

further purification. In this procedure, we placed 0.97 g of Mg $(NO_3)_2{\cdot}6H_2O$ and 4.04 g of Fe $(NO_3)_3{\cdot}9H_2O$ in a beaker containing 50 ml DDW and stirred for 30 min; we obtained a clear yellow solution that would be predicted to be a magnesium ferrites solution. Then, separately, we dissolved 3 g PEG in 20 ml DDW and stirred for 20 min, at 30 °C. The resulting solutions were mixed well at room temperature, then stirred continuously for 2 h at 60 °C to form a gel. The obtained gel of the PEG/Mg ferrite and the Mg ferrite solution were both transferred into an oven at 70 °C for 9 h to enhance the complete drying of the samples, after which the dry, solid brown crystals were transferred into a vacuum tube oven for calcination at 400 °C for 2 h, respectively. These procedures were repeated for 6 g PEG with the composition listed in Table 1. The Mg ferrite sample prepared was named T_1 and the 3 and 6 g PEG doped samples were named T_2 and T_3, respectively. The formulated samples were characterized using X-ray diffraction (XRD) spectroscopy (XRD-6000, Shimadzu Co., Japan). CuK_α radiation (0.154 nm) was used to analyze the samples at room temperature between 20° and 70° 2θ. Characterization of the morphology of the samples was conducted using scanning electron microscopy (SEM) using a SEM1010 SEM instrument (JEOL, Ltd, Japan). The EDX attached to the SEM microscope was used to determine the elemental compositions of the samples. An FTIR (FTIR-1650, PerkinElmer Co., USA) model spectrometer was used in the range of 4000–500 cm^{-1}. Thermogravimetric analysis (TGA) was done with a TGA-60H thermal analyzer (Shimadzu Co., Japan) in the temperature range of 49–995 °C at the heating rate of 20 °C per min. under nitrogen atmosphere, was used to characterize the thermal degradation properties. UV–visible diffuse reflectance spectroscopy (UV-DRS) (UV-3600, Shimadzu Co., Japan) was used to characterize the absorbance and the reflectance properties, and a vibrating sample magnetometer (VSM) Quantum design, (VSM-4700, model) Versalab Lake Shore Co. Ltd., USA measurements was done in the range of ±20 KOe to characterize the magnetic properties of the samples.

3. Results and discussion of properties of the MgFNPs and PEG-MgFNPs

3.1. Thermogravimetric study of PEG-MgFNPs

The thermal stability of the previously calcinated samples was determined using TGA by heating to 1000 °C at 10 °C/min, as shown in Fig. 1. The figure revealed that the decomposition of the sample occurred in several stages. In the first stage, 15% weight loss was recorded, as a result of the evaporation of water molecules. The second stage involved 10% weight loss, ascribed to removing the phytochemical moieties, and the third stage involved 12% weight loss which we ascribed to the complete removal of the phytochemical moieties, after which no further weight loss was recorded. Hence, the

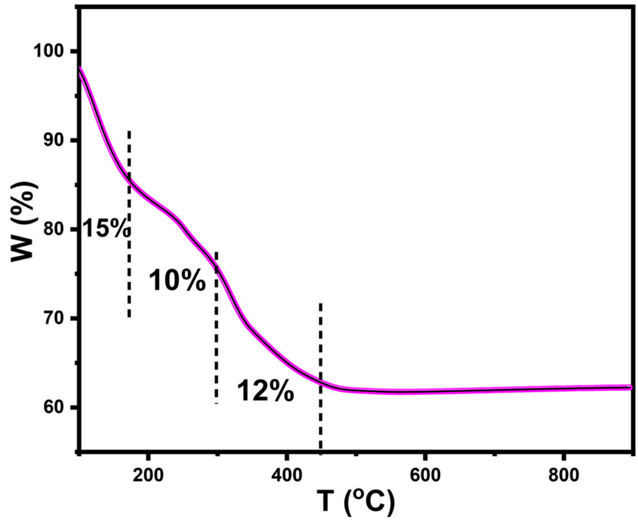

Figure 1. Thermogravimetric analysis of thermal stability of T_3 (6g-PEG-MgFNPs).

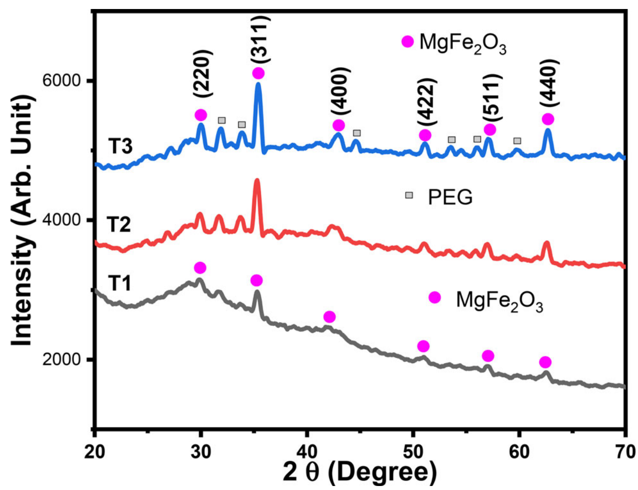

Figure 2. XRD spectra of the samples T_1, T_2, and T_3.

prior calcination process resulted in further increase in the decomposition of the sample during heating to 400 °C.

3.1. XRD study of MgFNPs and PEG-MgFNPs

The structural properties of the synthesized spinel nanoparticles were investigated by X-ray diffraction, as shown in Fig. 2. The diffraction peaks at the 2θ values shown were in agreement with the JCPDS card no. 36-0398 for Fe_2O_3. The most prominent peaks at the angles listed correspond to the $MgFe_2O_3$ crystallographic planes 220 (29.9°), 311 (35.3°), 400 (43.0°), 422 (51.0°), 511 (56.9°), and 440 (62.5°). The estimated crystallite sizes (D) of the $MgFe_2O_3$, normal to the 311 plane, based on the Debye–Scherer's equation (Eq. 1), are presented in Table 2.

Table 2. Crystallite size, Raman modes, and the saturation magnetization.

			Raman peaks (cm^{-1})		
Sample	D (nm)	M_s (emu/g)	A_1g	T_{2g} (2)	E_g
T_1	16.6	32.3	700.5	469.8	311.8
T_2	73.2	30.4	724.4	476.6	317.1
T_3	91.1	27.1	710.8	476.6	317.1

$$D = \frac{K\lambda}{\beta\cos\theta}, \quad (1)$$

where K is a constant ≈0.9, λ is the X-ray wavelength ($\lambda = 1.5406$ Å), β is the full width at half maximum (FWHM) of the X-ray diffraction peaks, and θ is the Bragg diffraction angle in degrees.[29] It can be concluded that the intensity and the size of the $MgFe_2O_3$ peaks increased with increasing the concentration of PEG, the PEG apparently enhancing the crystallinity and the crystal size of the $MgFe_2O_3$.

3.2. SEM study of MgFNPs and PEG-MgFNPs

Scanning electron microscopy (SEM) was used to analyze the particle morphology, as illustrated in Fig. 3a–c. The images showed particles of near spherical shape in the nano-size range. We observed an increase in the particle size as the concentration of PEG was increased. The particles in Fig 3a were of near uniform size and were distributed throughout the micrograph with low agglomeration. The PEG enhanced the binding of the nanoparticles, as observed in Fig. 3b,c. We observed an increase in the particle size as the PEG crystallite size increased. Energy-dispersive X-ray (EDX) spectroscopy attached to the SEM was used to analyze the elemental chemical composition of the synthesized nanoparticles. Figure 3d shows the EDX spectra of the as-prepared magnesium ferrite showing the constituent elements. The EDX spectra of the sample had the highest peaks for Mg, Fe, and O; they also showed a small impurity peak of Na for the as-prepared sample without the PEG. However, the Na impurity peak was less with the addition of PEG, as shown in Fig. 3e,f.

3.3. Optical study of MgFNPs and PEG-MgFNPs

The reflectance and the energy bandgap of the samples were investigated using UV-DRS. UV-DRS has great advantages in studying the optical properties of powder materials from their absorbance spectra in the visible range. The reflectance of the samples is presented in Fig. 4a. The reflectance data was converted using the Kubelka–Munk (KM) relation theory to obtain the absorption coefficient (α) as presented in Eq. (2).[30,31]

$$F(R) = \frac{\alpha}{s} = \frac{(1-R)^n}{2R}, \quad (2)$$

where $F(R)$ is the KM function.

$$\alpha = (1-R)^n (\text{molar absorption coefficient}).$$

$s = 2R$ (scattering factor).

$R = \frac{\%R}{100}$ (reflectance of materials).

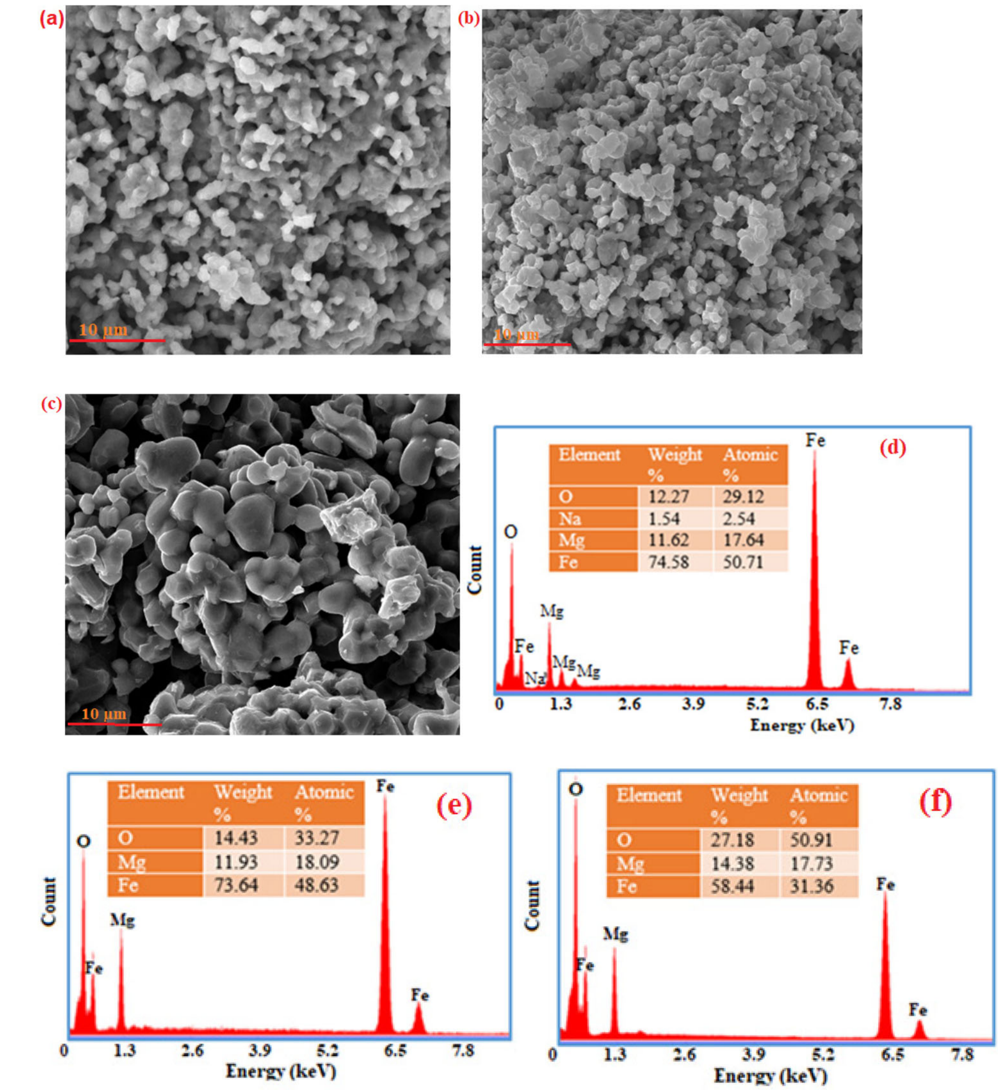

Figure 3. (a–c) SEM images of T_1, T_2, and T_3 and (d–f) EDX images of T_1, T_2, and T_3 samples.

The energy bandgaps (E_gs) were calculated from the relationship between the KM relation theory and the Tauc plot, as expressed in Eqs. (2) and (3). The direct allowed energy transitions of the samples, as shown in Fig. 4b–d, were obtained through extrapolation of the Tauc plot, as shown in the figures, to $(\alpha h\nu)^2 \approx 0$.

$$(\alpha h\nu)^n = A\left(h\nu - E_g\right). \tag{3}$$

In Eq. (2), $F(R)$ is proportional to α since s is only dependent on the wavelength. Hence, the energy bandgaps of the samples were obtained from $(\alpha h\nu)^2$ vs. $h\nu$ plots by using the Tauc's relation (Eq. 3).[30,31] Studies have shown that a doping agent greatly influences the energy bandgap of materials.[32,33] Hence, the decrease in the E_g from 3.35 to 2.88 eV, as shown in Fig. 4b–d, is due to the increase in PEG concentration.

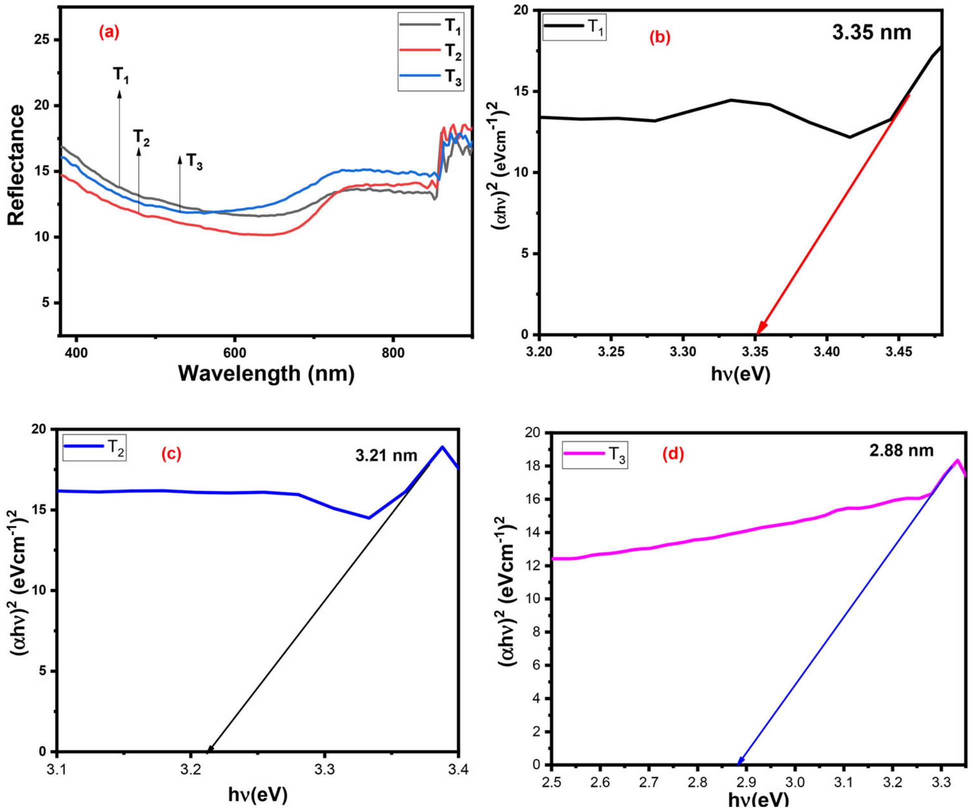

Figure 4. Reflectance and energy bandgap of the samples T_1, T_2, and T_3.

3.4. Raman study of MgFNPs and PEG-MgFNPs

The Raman spectra results, as shown in Fig. 5, gives information on the vibration modes associated with the atomic structure and the symmetry of the samples.[34] The A1g and E_g modes are related to the symmetric stretching and bending of the oxygen anions in MgFNPs, respectively, whereas the $T2_g$ mode is associated with the asymmetric stretching of the oxygen anions in the tetrahedral A-sites and the octahedral B-sites cations.[35] In Fig. 5, four clear Raman bands can be seen for the curve with the addition of different concentrations of PEG, which altered the Raman bands position of the sample. As shown, there were changes in the relative intensities and positions of the peaks with increasing the concentration of PEG. As shown in Table 1 and Fig. 5, the Raman band between 704 and 712 cm^{-1} is assigned to the A1g band, which is due to the Fe–O's stretching vibrations in tetrahedral sites. The Raman band between 469 and 473 cm^{-1} wavenumbers was assigned to the T_{2g} (2), the band between 298 and 309 cm^{-1} was assigned to E_g and the band between 1300 and 1350 cm^{-1} was assigned to the D-band band. An increase to the same higher wavenumbers was observed for the T_{2g} (2), E_g, and A_{1g} bands with the addition of 3 and 6 g of PEG to the sample, as presented in Table 2. Raman bands shifts were observed in all the samples with the addition of PEG. In addition, the addition of PEG decreased the intensity of the peaks in the Raman spectra.

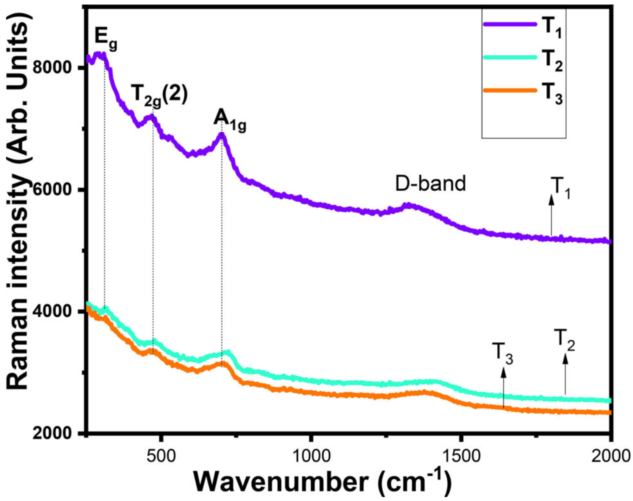

Figure 5. Raman spectra of the samples T_1, T_2, and T_3.

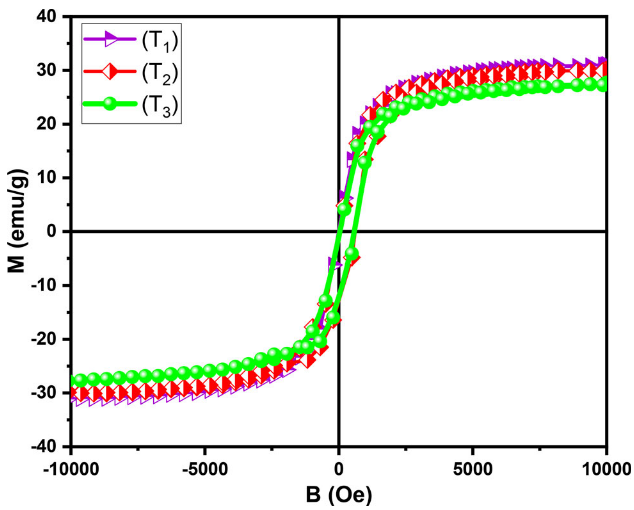

Figure 6. Magnetic properties of the samples T_1, T_2, and T_3.

3.5. Magnetic properties study of MgFNPs and PEG-MgFNPs

The hysteresis loops of the obtained samples were determined using a vibrating sample magnetometer. The loop of magnetization against the magnetic field, as shown in Fig. 6, shows the effect of PEG on the magnetic properties of the samples. All the samples exhibited a ferromagnetic nature, as seen in Fig 6. The saturation magnetization (M_s), as presented in Table 2, decreased as the amount of PEG increased. We presume the decrease in M_s should be attributed to the cation site distribution associated with the spinel ferrite structure or the decrease in the Fe content in the material as PEG increases. Hence, the PEG concentration influenced the decrease in the M_s in the magnetic properties of the samples.

4. Conclusions

The properties of MgFNPs and PEG-MgFNPs prepared via a bio-inspired synthesis protocol, using PEG as a potential capping agent to tailor the microstructural properties of the sample, were successfully determined. The characterization via TGA, XRD, SEM, DRS, and VSM showed the effect of PEG on the samples. The XRD gave a crystallite size increasing from 16 nm for the MgFNPs to 90 nm for the PEG- MgFNPs with 6.0 g of PEG. In addition an increase in the crystallinity of the sample was observed due to the PEG. The SEM images showed a spherical morphology for all the samples, with enhanced particle size with increasing PEG. The Raman band intensity decreased as the PEG concentration increased. The magnetic properties had a ferromagnetic nature with reduced saturation magnetization as the PEG increased. It is noteworthy that the PEG concentration influenced the desirable properties of the sample, enhancing their suitability for biomedical applications; with the most desirable being the sample with 6 g PEG.

Acknowledgments

Samson O. Aisida expresses his appreciation to Prof. Ishaq Ahmad, the director of the Experimental Physics Lab., National Center for Physics, Islamabad, Pakistan and Prof. Fabian I. Ezema, Department of Physics and Astronomy University of Nigeria, for their assistance to access some characterization instruments for the success of this work.

Disclosure statement

No potential conflict of interest was reported by the author(s).

Funding

Samson O. Aisida and Fabian I. Ezema acknowledge support from the TETFUND under the contract entitled (TETFUND/DR&D/CE/UNI/NSKKA/RP/VOL.1). Samson O. Aisida acknowledges the NCP-TWAS Postdoc Fellowship award (NCP-CAAD/TWAS_Fellow8408).

References

[1] Silva, G. A. Introduction to Nanotechnology and Its Applications to Medicine. *Surg. Neurol.* **2004**, *61*, 216–220. DOI: 10.1016/j.surneu.2003.09.036.

[2] Verma, S.; Joy, P.; Khollam, Y.; Potdar, H.; Deshpande, S. Synthesis of Nanosized $MgFe_2O_4$ Powders by Microwave Hydrothermal Method. *Mater. Lett.* **2004**, *58*, 1092–1095. DOI: 10.1016/j.matlet.2003.08.025.

[3] Shimizu, Y.; Arai, H.; Seiyama, T. Theoretical Studies on the Impedance Humidity Characteristics of Ceramic Humidity Sensors. *Sens. Actuators* **1985**, *7*, 11–22. DOI: 10.1016/0250-6874(85)87002-5.

[4] Han, X.; Tian, P.; Pang, H.; Song, Q.; Ning, G.; Yu, Y.; Fang, H. Facile Synthesis of Magnetic Hierarchical MgO-$MgFe_2O_4$ Composites and Their Adsorption Performance towards Congo Red. *RSC Adv.* **2014**, *4*, 28119–28125. DOI: 10.1039/C4RA02313G.

[5] Godbole, R.; Rao, P.; Alegaonkar, P.; Bhagwat, S. Influence of Fuel to Oxidizer Ratio on LPG Sensing Performance of $MgFe_2O_4$ Nanoparticles. *Mater. Chem. Phys.* **2015**, *161*, 96–106. DOI: 10.1016/j.matchemphys.2015.05.028.

[6] Edmilson, M. M.; Renato, V. G.; Renato, F. J.; Pedro, K. K.; Liane, M. R.; Marco, A. G. Gold Nanoparticles Supported on Magnesium Ferrite and Magnesium Oxide for the Selective Oxidation of Benzyl Alcohol. *RSC Adv.* **2015**, *5*, 150. DOI: 10.1039/C4RA16159A.

[7] Shahid, M.; Jingling, L.; Ali, Z.; Shakir, I.; Warsi, M. F.; Parveen, R.; Nadeem, M. Photocatalytic Degradation of Methylene Blue on Magnetically Separable $MgFe_2O_4$ under Visible Light Irradiation. *Mater. Chem. Phys.* **2013**, *139*, 566–571. DOI: 10.1016/j.matchemphys.2013.01.058.

[8] Yang, G.-f.; Li, X.-h.; Zhao, Z.; Wang, W.-b. Preparation, Characterization, In Vivo and In Vitro Studies of Arsenic Trioxide Mg-Fe Ferrite Magnetic Nanoparticles. *Acta Pharmacol. Sin.* **2009**, *30*, 1688–1693. DOI: 10.1038/aps.2009.158.

[9] Chen, Q.; Zhang, Z. J. Size Dependent Superparamagnetic Properties of $MgFe_2O_4$ Spinel Ferrite Nanocrystallites. *Appl. Phys. Lett.* **1998**, *73*, 3156–3158. DOI: 10.1063/1.122704.

[10] Liu, Y.; Liu, Z.; Yang, Y.; Yang, H.; Shen, G.; Yu, R. Simple Synthesis of $MgFe_2O_4$ Nanoparticles as Gas Sensing Materials. *Sens. Actuators B* **2005**, *107*, 600–604. DOI: 10.1016/j.snb.2004.11.026.

[11] Haw, C.; Mohamed, F.; Chia, C.; Radiman, S.; Zakaria, S.; Huang, N.; Lim, H. Hydrothermal Synthesis of Magnetite Nanoparticles as MRI Contrast Agents. *Ceram. Int.* **2010**, *36*, 1417–1422. DOI: 10.1016/j.ceramint.2010.02.005.

[12] Franco, J.; Silva, M. S. High Temperature Magnetic Properties of Magnesium Ferrite Nanoparticles. *J. Appl. Phys.* **2011**, *109*, 07B505-3. DOI: 10.1063/1.3536790.

[13] Lou, Z.; He, M.; Wang, R.; Qin, W.; Zhao, D.; Chen, C. Large-Scale Synthesis of Monodisperse Magnesium Ferrite via an Environmentally Friendly Molten Salt Route. *Inorg. Chem.* **2014**, *53*, 2053–2057. DOI: 10.1021/ic402558t.

[14] Turkin, A.; Drebushcha, V. Synthesis and Calorimetric Investigation of Stoichiometric Fe-Spinels: $MgFe_2O_4$. *J. Cryst. Growth* **2004**, *265*, 165–167. DOI: 10.1016/j.jcrysgro.2004.01.037.

[15] Kulkarn, R.; Joshi, H. Comparison of Magnetic Properties of $MgFe_2O_4$ Prepared by Wet-Chemical and Ceramic Methods. *J. Solid State Chem.* **1986**, *64*, 141–147. DOI: 10.1016/0022-4596(86)90133-7.

[16] Patil, J.; Mulla, I.; Suryavanshi, S. Gas Response Properties of Citrate Gel Synthesized Nanocrystalline $MgFe_2O_4$: Effect of Sintering Temperature. *Mater. Res. Bull.* **2013**, *48*, 778–784. DOI: 10.1016/j.materresbull.2012.11.060.

[17] Koferstein, R.; Walther, T.; Hesse, D.; Ebbinghaus, S. Preparation and Characterization of Nanosized Magnesium Ferrite Powders by a Starch-Gel Process and Corresponding Ceramics. *J. Mater. Sci.* **2013**, *48*, 6509–6518. DOI: 10.1007/s10853-013-7447-x.

[18] Hussein, S.; Elkady, A.; Rashad, M.; Mostafa, A.; Megahid, R. Structural and Magnetic Properties of Magnesium Ferrite Nanoparticles Prepared via EDTA-Based Sol-Gel Reaction. *J. Magn. Magn. Mater.* **2015**, *379*, 9–15. DOI: 10.1016/j.jmmm.2014.11.079.

[19] Patil, J.; Khandeka, M.; Mulla, I.; Suryavanshi, S. Combustion Synthesis of Magnesium Ferrite as Liquid Petroleum Gas (LPG) Sensor: effect of Sintering Temperature. *Curr. Appl. Phys.* **2012**, *12*, 319–324. DOI: 10.1016/j.cap.2011.06.029.

[20] Dalt, S. D.; Takimi, A.; Sousa, V.; Bergmann, C. Magnetic and Structural Characterization of Nanostructured $MgFe_2O_4$ Synthesized by Combustion Reaction. *Part. Sci. Technol.* **2009**, *27*, 519–527. DOI: 10.1080/02726350903328662.

[21] Candeia, R.; Souza, M.; Bernardi, M.; Maestrelli, S.; Santos, I.; Souza, A.; Longo, E. $MgFe_2O_4$ Pigment Obtained at Low Temperature. *Mater. Res. Bull.* **2006**, *41*, 183–190. DOI: 10.1016/j.materresbull.2005.07.019.

[22] Chandradass, J.; Jadhav, A.; Kim, H. Surfactant Modified $MgFe_2O_4$ Nano Powders by Reverse Micelle Processing: effect of Water to Surfactant Ratio (R) on the Particle Size and Magnetic Property. *Appl. Surf. Sci.* **2012**, *258*, 3315–3320. DOI: 10.1016/j.apsusc.2011.11.092.

[23] Holec, P.; Plocek, J.; Nižňanský, D.; Vejpravová, J. Preparation of $MgFe_2O_4$ Nanoparticles by Microemulsion Method and Their Characterization. *J. Sol-Gel Sci. Technol.* **2009**, *51*, 301–305. DOI: 10.1016/j.jcrysgro.2005.03.038.

[24] Nonkumwong, J.; Ananta, S.; Jantaratana, P.; Phumying, S.; Maensiri, S.; Srisombat, L. Phase Formation, Morphology and Magnetic Properties of $MgFe_2O_4$ Nanoparticles Synthesized by Hydrothermal Technique. *J. Magn. Magn. Mater.* **2015**, *381*, 226–234. DOI: 10.1016/j.jmmm.2015.01.001.

[25] Ilhan, S.; Izotova, S.; Komlev, A. Synthesis and Characterization of $MgFe_2O_4$ Nanoparticles Prepared by Hydrothermal Decomposition of co-Precipitated Magnesium and Iron Hydroxides. *Ceram. Int.* **2015**, *41*, 577–585. DOI: 10.1016/j.ceramint.2014.08.106.

[26] Sasaki, T.; Ohara, S.; Naka, T.; Vejpravova, J.; Sechovsky, V.; Umetsu, M.; Takami, S.; Jeyadevan, B.; Adschiri, T. Continuous Synthesis of Fine $MgFe_2O_4$ Nanoparticles by Supercritical Hydrothermal Reaction. *J. Supercrit. Fluids* **2010**, *53*, 92–94. DOI: 10.1016/j.supflu.2009.11.005.

[27] Selvam, R.; Ramasamy, S.; Mohiyuddin, S.; Enoch, I. V.; Gopinath, P.; Filimonov, D. Molecular Encapsulator–Appended Poly(Vinyl Alcohol) Shroud on Ferrite Nanoparticles. Augmented Cancer–Drug Loading and Anticancer Property. *Mater. Sci. Eng. C* **2018**, *93*, 125–133. DOI: 10.1016/j.msec.2018.07.058.

[28] Zhang, X.; Wang, H.; Wen, X.; Zhang, A.; Wang, X.; Zhong, L.; Liu, C.; Sun, R. Synthesis and Characterization of Xylan Grafted with Polyethylene Glycol in Ionic Liquid and Their Use as Moisture-Absorption/Retention Biomaterials. *Macromol. Mater. Eng.* **2016**, *301*, 287–295. DOI: 10.1002/mame.201500377.

[29] Aisida, S. O.; Akpa, P. A.; Ahmad, I.; Maaza, M.; Ezema, F. I. Influence of PVA, PVP and PEG Doping on the Optical, Structural, Morphological and Magnetic Properties of Zinc Ferrite Nanoparticles Produced by Thermal Method. *Phys. B: Condens. Matter* **2019**, *571*, 130–136. DOI: 10.1016/j.physb.2019.07.001.

[30] Khan, J. A.; Qasim, M.; Singh, B. R.; Singh, S.; Shoeb, M.; Khan, W.; Das, D.; Naqvi, A. H. Synthesis and Characterization of Structural, Optical, Thermal and Dielectric Properties of Polyaniline/$CoFe_2O_4$ Nanocomposites with Special Reference to Photocatalytic Activity. *Spectrochim. Acta A Mol. Biomol. Spectrosc.* **2013**, *109*, 313–321. DOI: 10.1016/j.saa.2013.03.011.

[31] Sagar, E. S.; Patange, S.; Kadam, R.; Mane, M.; Jadhav, K. Structure Refinement, Cation Site Location, Spectral and Elastic Properties of Zn^{2+} Substituted $NiFe_2O_4$. *J. Mol. Struct.* **2012**, *1024*, 77–83. DOI: 10.1016/J.MOLSTRUC.2012.05.014.

[32] Tatarchuk, T. R.; Paliychuk, N. D.; Bououdina, M.; Al-Najar, B.; Pacia, M.; Macyk, W.; Shyichuk, A. Effect of Cobalt Substitution on Structural, Elastic, Magnetic and Optical Properties of Zinc Ferrite Nanoparticles. *J. Alloys Compd.* **2018**, *731*, 1256–1266. DOI: 10.1016/j.jallcom.2017.10.103.

[33] Beltran, J. J.; Barrero, C. A.; Punnoose, A. Understanding the Role of Iron in the Magnetism of Fe Doped ZnO Nanoparticles. *Phys. Chem. Chem. Phys.* **2015**, *17*, 15284–15296. DOI: 10.1039/C5CP01408E.

[34] Baraliya, J. D.; Joshi, H. H. Spectroscopy Investigation of Nanometric Cobalt Ferrite Synthesized by Different Techniques. *Vib. Spectrosc.* **2014**, *74*, 75–80. DOI: 10.1016/j.vibspec.2014.07.013.

[35] Yu, T.; Shen, Z.; Shi, Y.; Ding, J. Cation Migration and Magnetic Ordering in Spinel $CoFe_2O_4$ Powder: Micro-Raman Scattering Study. *J. Phys.: Condens. Matter* **2002**, *14*, L613. DOI: 10.1088/0953-8984/14/37/101.